Reflectance anisotropy spectroscopy of Fe_3O_4(110): Anisotropic strain

B. Walls,* K. Fleischer, K. Zhussupbekov, O. Lübben, K. Walshe, and I. V. Shvets
School of Physics and Centre for Research on Adaptive Nanostructures and Nanodevices, Trinity College Dublin, Dublin 2, Ireland

(Received 15 May 2018; published 26 July 2018)

We present a study of (110)-terminated magnetite using a range of surface-sensitive techniques, the foremost of those being reflectance anisotropy spectroscopy (RAS). The anisotropic optical response of the as-polished and row-reconstructed terminations are investigated. The responses are interpreted to result from termination-induced anisotropic shifts in energy of the bulklike optical transitions. Density functional theory (DFT) calculations demonstrate that the row reconstruction of Fe_3O_4(110) exhibits anisotropic strain in its terminating layers, and this strain is concluded to be the origin of the RAS response. X-ray photoelectron spectroscopy measurements demonstrate that the row reconstruction is reduced and the stoichiometry in the surface region is relatively easily altered by *in situ* preparation procedures. This is correlated to altered surface electronic properties identified by scanning tunneling spectroscopy measurements. RAS is sensitive to this change in surface structure, with the magnitude of the RAS response being altered.

DOI: 10.1103/PhysRevB.98.045428

I. INTRODUCTION

Magnetite (Fe_3O_4) is a half-metallic conductor [1,2] and a high-Curie-temperature (838 K) ferrimagnet, and it undergoes a Verwey transition at around 120 K [3,4]. It is utilized as a catalyst in processes such as hydrogenation [5], the water-gas-shift reaction [6], and ammonia synthesis [7], to name but a few. Fe_3O_4 exists in an inverse spinel crystal structure. Iron atoms are divalent or trivalent and occupy octahedral (Fe_{oct}) or tetrahedral (Fe_{tet}) coordinates. The distribution of electrons and a relatively complex crystal structure lead to all three low-index Fe_3O_4 surfaces, (001), (110), and (111), being polar. The need to compensate for this polarity and the ease at which preparation procedures alter the stoichiometry result in a range of complex surface reconstructions [8–10]. Fe_3O_4's (001) and (111) surfaces have been utilized as templates for nanostructure growth [8,11], the study of single-atom catalysis, and single-atom/-molecule absorption dynamics [12–16]. The (110) termination, which exhibits a one-dimensional row reconstruction [10,17,18], represents a potential template for one-dimensional nanostructure growth.

Reflectance anisotropy spectroscopy (RAS) is a nondestructive optical technique which probes the optical anisotropy of a surface region in the plane of the termination. This is achieved by illuminating the sample with linearly polarized light at near-normal incidence and measuring the difference in reflectance from two orthogonal surface directions. Isotropic and amorphous materials as well as anisotropic materials with randomly orientated domains will not exhibit a RAS signal. Even in the case of (110)-terminated cubic materials, which are terminated by anisotropic planes, the stacking of orthogonal planes in the bulk results in the signal of individual planes canceling. However, the symmetry-breaking surface can lead to the inequivalence of the terminating planes and the underlying orthogonal bulklike planes, resulting in a nonzero cancellation. In such cases, the RAS signal is due to surface states of the anisotropic termination and/or its influence on the bulklike region in the vicinity of the termination.

The initial and majority of RAS studies have been conducted on semiconducting surfaces [19–21]; the technique has been utilized to investigate semiconductor surface reconstructions and to monitor the growth of epitaxially grown semiconductor surfaces. Furthermore, the structure of metal absorbates on metal and semiconductor surfaces or the absorbent-induced reconstruction of the substrate has received considerable attention [19,22–26]. RAS represents a technique which can characterize surface and electronic structure, identify specific surface terminations, and monitor changes in surface structure in real time. Despite this RAS studies of metal oxides have received little attention; wide-band-gap ZnO [27], *ex situ* as-polished Fe_3O_4(110) [28], and superconducting cuprates [29] have been investigated. Recently, we showed that RAS is sensitive to different surface terminations of $SrTiO_3$(110) [30]. The response in the ultraviolet, above the optical band gap, resulted from surface-induced strain.

Here we present a RAS study of Fe_3O_4(110), which is complemented by a range of surface-sensitive techniques, to further understand the optical response of metal oxide surface reconstructions. In doing so we shed light on aspects of the {111}-nanofaceted row reconstruction of Fe_3O_4(110). First, the *ex situ* as-polished surface, presented previously by Fleischer *et al.* [28], is briefly returned to. Subsequently, the influence of *in situ* ultrahigh-vacuum (UHV) annealing on the RAS response is discussed. Last, the spectra of the Fe_3O_4(110) {111}-nanofaceted row reconstruction is examined at length. The optical responses are interpreted to originate from anisotropic strain in the surface region.

II. THEORY

In RAS measurements the difference in the reflectance from the two orthogonal surface directions (x, y) is normalized to

*wallsb@tcd.ie

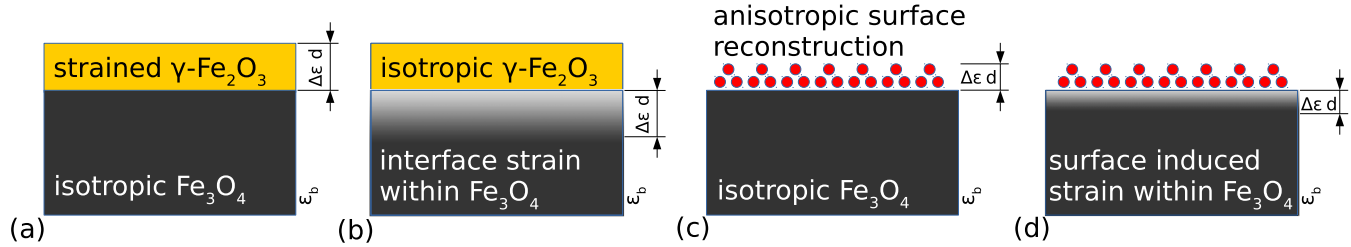

FIG. 1. Potential sources of optical anisotropy for Fe_3O_4(110). (a) and (b) illustrate the potential sources in the presence of a maghemite (γ-Fe_2O_3) overlayer, which forms in the ambient and hence is expected for the as-polished crystal: (a) anisotropic strain in a γ-Fe_2O_3 overlayer and (b) anisotropic strain in Fe_3O_4 due to the γ-Fe_2O_3-Fe_3O_4 interface. $\Delta\epsilon d$ illustrates the region which generates the optical anisotropy (see discussion in Sec. II). (c) illustrates the optical anisotropy generated by an anisotropic Fe_3O_4 surface reconstruction (the schematic depicts the dominant row reconstruction), while (d) illustrates anisotropic strain in the underlying Fe_3O_4 due to the row reconstruction. (c) and (d) can be expected in the case of the clean *in situ* UHV annealed crystal.

the average reflectance:

$$\frac{\Delta r}{r} = 2\frac{r_x - r_y}{r_x + r_y} \tag{1}$$

The reflectance anisotropy can be related to the dielectric function of the bulk and surface region. McIntyre and Aspnes initially developed the three-phase model to determine the change in reflectivity when a thin film, in contact with the ambient, was grown on a bulk substrate [31]. Aspnes later employed the three-phase model to describe the difference in reflectivity of p-polarized light from two orthogonal directions perpendicular to the surface normal [32]. Considering light wavelengths far greater than the depth of the surface region d, which is distinguishable from the underlying bulk, the RAS unit is expressed as [19]

$$\frac{\Delta r}{r} = \frac{4\pi d i}{\lambda}\frac{\Delta\epsilon}{\epsilon_b - 1}. \tag{2}$$

Here $\Delta\epsilon = \epsilon_x - \epsilon_y$, with ϵ_x and ϵ_y being two orthogonal surface dielectric functions. ϵ_b is the complex dielectric function of the underlying bulk, and the RAS unit is a complex quantity.

If the orthogonal components of the surface region's dielectric function, ϵ_x and ϵ_y, are similar in magnitude but differ slightly in broadening and/or energy shifts due to, for example, anisotropic strain [33], the three-layer model can be used with $\Delta\epsilon$ expressed as the first energy derivative of ϵ_b. Replacing $\Delta\epsilon$ with $\frac{d\epsilon_b}{dE}$ in Eq. (2) and extracting the real component, which is presented throughout this work, by taking the complex conjugate, we obtain the following expression:

$$\mathrm{Re}\left(\frac{\Delta r}{r}\right) = \frac{4\pi d}{\lambda}\frac{(\epsilon^{'} - 1)\frac{d\epsilon^{''}}{dE} - \epsilon^{''}\frac{d\epsilon^{'}}{dE}}{(\epsilon^{'} - 1)^2 + (\epsilon^{''})^2}, \tag{3}$$

with $\epsilon_b = \epsilon^{'} + i\epsilon^{''}$. One must keep in mind that this expression is valid only for the transitions in the vicinity of a single critical point. Optical anisotropies originating from the modification of different states can produce signals of different widths, signs, and magnitudes. Optical anisotropies of cubic, and hence bulk isotropic, materials are generated in the surface region by crystal field, electric field, or strain anisotropies generated by surface relaxation and/or oxidation. Considering the intrinsic anisotropy of the cubic (110) termination and the nature of the dominant one-dimensional faceted surface reconstruction of Fe_3O_4(110), the RAS spectra are discussed in terms of anisotropic strain in the surface region. Henceforth, Eq. (3) will be referred to as the strain model. In the case of the as-polished surface the optical anisotropy of a maghemite (γ-Fe_2O_3) overlayer, which forms in ambient conditions [34], or this overlayer's influence on the underlying Fe_3O_4 must be considered.

Figure 1 illustrates the potential sources of optical anisotropy for Fe_3O_4(110). In the case of the as-polished surface optical anisotropy can be due to a strained γ-Fe_2O_3 surface layer [Fig. 1(a)] and/or anisotropic strain of Fe_3O_4 in the vicinity of the γ-Fe_2O_3-Fe_3O_4 interface [Fig. 1(b)]. Anisotropy of the clean surface, which is formed by high-temperature annealing in vacuum, can be due to an anisotropic surface state of the dominant row reconstruction [Fig. 1(c)] and/or its influence on the immediately underlying Fe_3O_4 bulk [Fig. 1(d)]. The strain model can be used to qualitatively examine the cases in Figs. 1(a) and 1(d) and can provide an approximation for Fig. 1(b), in which a full solution requires four layers. Figure 1(c) requires knowledge of the row-reconstruction atomic structure, which remains uncharacterized, and in-depth DFT calculations to determine its contribution to the RAS signal.

III. EXPERIMENTAL DETAILS

Measurements have been performed across two chambers, a scanning tunneling microscopy (STM) chamber and an x-ray photoelectron spectroscopy (XPS) chamber. The microscope used in this work is a commercial low-temperature slider-type STM from Createc. All images presented were obtained in constant-current mode at 77 K. The STM tips used were [001]-oriented single-crystalline tungsten, which were electrochemically etched in NaOH. The bias is applied to the sample with respect to the tip. XPS measurements have been performed using a laboratory-based Omicron MultiProbe-XPS system using monochromated Al-K x rays ($hf = 1486.7$ eV). *In situ* RAS measurements are made possible by a strain-free fused quartz window on the STM chamber. The sample cannot be rotated in the plane perpendicular to the light propagation direction, and hence, a photoelastic modulator allows for measurement of the optical anisotropy. The spectrometer used in this work, which has a spectral range of 0.8–5.5 eV, is described

in [35]. In the presented RAS spectra x and y in Eq. (1) correspond to the [001] and [$\bar{1}$10] directions, respectively. This is the same formalism as in [28].

The surface of a (110)-orientated Fe_3O_4 single crystal (Moscow State Steel and Alloys Institute) was initially polished using sandpaper. Subsequently, diamond and cerium oxide suspensions with a final grain size of 0.01 μm were used for further polishing until an optically flat surface was achieved. During the polishing process, the sample was moved in a figure-of-eight pattern and rotated occasionally in order to ensure that the polishing was smooth and did not cause any preferential direction which might influence any measurement of the sample's anisotropy.

Annealing (110)-terminated thin-film or single-crystalline Fe_3O_4 in oxygen [10] or UHV [10,18,36,37] environments results in the formation of a (1×3) row-reconstructed termination. Recently, Parkinson *et al.* [10] concluded that the reconstruction was a result of periodic nanofaceting which exposed {111}-like planes; the reconstruction consists of rows with troughs in between, and the slope from ridge to trough was concluded to be a {111}-type plane, which is energetically favorable. On the basis of XPS and minor differences in low-energy electron diffraction (LEED), it was noted that the oxygen- and UHV-annealed crystals likely exhibit different surface structures. Here we investigate these difference in detail.

IV. RESULTS

A. Polished surface

The RAS spectra of the as-polished crystal are identical to those reported in [28] and are depicted in Fig. 2 (solid line). The anisotropic optical response in [28] was suggested to originate from anisotropic strain; the line shape resembled the first energy derivative of Fe_3O_4's dielectric function, indicating that small shifts in energy of the optical transitions, such as those associated with anisotropic strain, were likely responsible for the anisotropic response. However, the possibility that a thin γ-Fe_2O_3 overlayer may contribute to the anisotropic response was not ruled out.

Here the crystal has been UHV annealed *in situ* stepwise at 200 °C, 350 °C, 550 °C, and 800 °C. The RAS spectra for each of these steps are depicted in Fig. 2 alongside that of the as-polished surface. Each anneal step reduces the magnitude of the large derivativelike feature. The line shape remains largely the same, although the maxima and minima located at 1.1 and 1.6 eV are progressively shifted to lower energies. The spectra after heating up to 800 °C show the greatest deviation from the as-polished surface line shape; the maximum at 2.3 eV is removed entirely, and a broad feature at around 3.3 eV is enhanced.

In ambient conditions the Fe_3O_4 surface region is transformed into γ-Fe_2O_3 [34]. However, in an extremely low molecular oxygen partial pressure environment, such as UHV, Fe_3O_4 is the stable iron oxide above approximately 600 °C [41]. The penetration depth of light for Fe_3O_4 varies from just 30 nm in the ultraviolet to a maximum of 160 nm around 1.4 eV [28]. Hence, considering that after prolonged exposure (2 months) the γ-Fe_2O_3 overlayer formed on thin-film Fe_3O_4

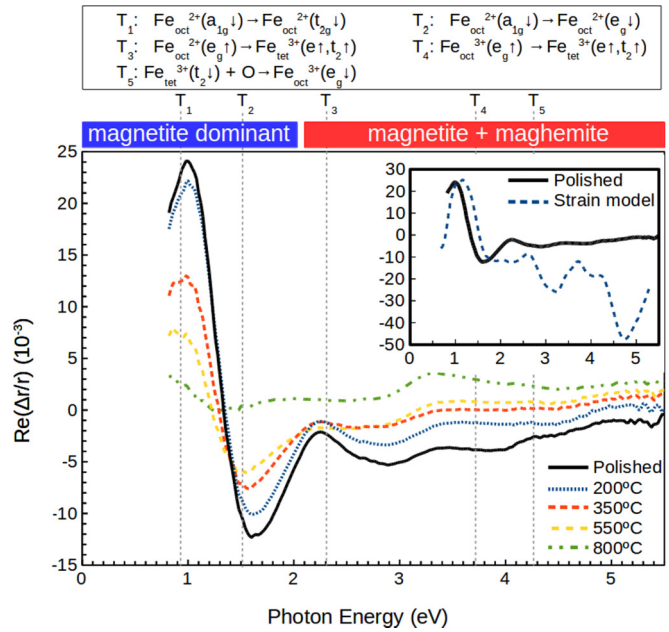

FIG. 2. RAS of the as-polished surface (solid line). The crystal was annealed progressively at increasing temperatures in a UHV environment. Clearly, the magnitude of the maxima-minima feature is progressively reduced with each anneal step. The comparison (inset) between the as-polished RAS line shape (solid line) and the Fe_3O_4 strain model (dashed line) in the spectral region below around 2 eV indicates a modification of Fe_3O_4's bulklike states. ϵ_b, which is used to calculate the strain model, is taken from experimental work conducted by Schlegel and Wachter [38]. Vertical dashed lines denote energy positions of Fe_3O_4's optical transitions taken from [39,40].

is only 2 nm [34], RAS will probe both anisotropies in the γ-Fe_2O_3 overlayer and the underlying Fe_3O_4.

The vertical dashed lines in Fig. 2 signify energetic positions of Fe_3O_4's optical transitions, taken from [39,40]. Due to the lack of detailed studies of γ-Fe_2O_3's optical transitions, only Fe_3O_4's optical transitions are depicted. All Fe_3O_4 optical transitions probed by RAS are interband, as intraband transitions of Fe_3O_4 are below 0.2 eV [40]. Therefore, the complex interband transitions of Fe_3O_4 will give rise to broad features. The line shape of the as-polished surface exhibits a relatively broad derivativelike feature below around 2.0 eV, with the peaks in the vicinity of the optical transitions. This indicates a surface-induced modification of Fe_3O_4's bulklike states is the origin of the RAS signal for bulk isotropic Fe_3O_4. The inset of Fig. 2 depicts the Fe_3O_4 strain model (dashed line) calculated from Eq. (3), which is compared to the as-polished RAS line shape (solid line). ϵ_b for Fe_3O_4 is taken from experimental work conducted by Schlegel and Wachter [38] in which the dielectric function has been obtained by the means of a Kramers-Kronig analysis of the reflectivity spectrum. A value for d of 22 nm was chosen to fit the maxima-minima feature. The line shape is in good agreement at low energies with the maxima-minima feature reproduced. This derivativelike structure below 2.0 eV cannot be attributed to a γ-Fe_2O_3 overlayer as γ-Fe_2O_3 has a band gap of 2.0 eV [42,43]. Indeed, optical transitions below 2.0 eV in Fe_3O_4 are known to involve only Fe^{2+}_{oct} sites [39,40], and γ-Fe_2O_3 contains Fe_{oct} vacancies, which results in the

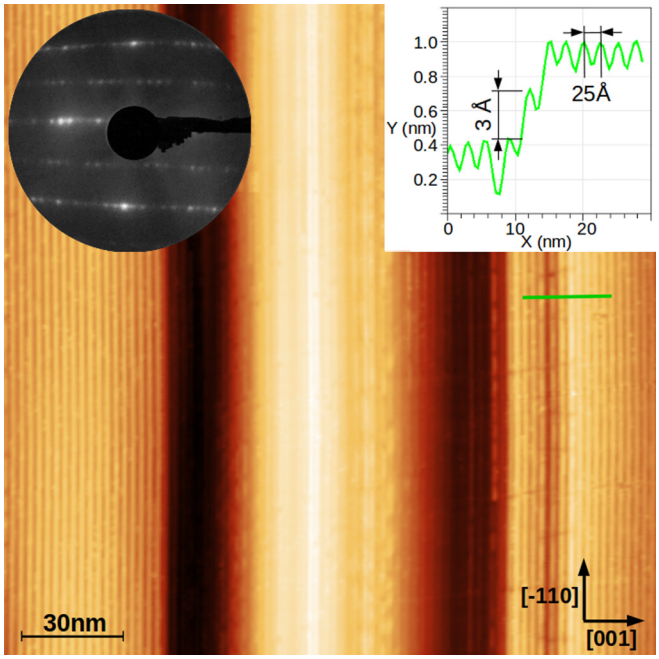

FIG. 3. Here 200 × 200 nm^2, $V = 1.2$ V, and $I = 0.19$ nA. The same surface on which RAS measurements, depicted in Fig. 4, were performed. The line profile illustrating a row periodicity of 25 Å and a step height of 3 Å is indicative of the {111}-nanofaceted row reconstruction of Fe_3O_4(110) [10].

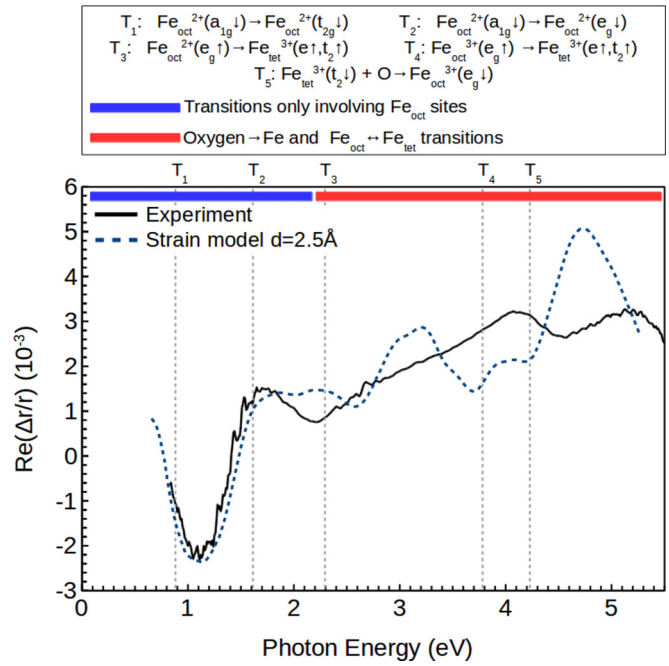

FIG. 4. RAS of the {111}-nanofaceted row reconstruction of Fe_3O_4(110) (solid line). The surface was prepared by two 10-s UHV flash anneals at 900 °C. Vertical dashed lines denote energy positions of Fe_3O_4's optical transitions taken from [39,40]. Below around 2.0 eV, transitions involve only Fe_{oct} sites, while above around 2.0 eV oxygen and Fe_{tet} sites are also involved. The strain model (dashed line) reproduces the minima-maxima feature in the infrared.

absence of the Fe^{2+}_{oct} site. The comparable electronic structures of Fe_3O_4 and γ-Fe_2O_3, both of which are inverse spinel, will likely result in RAS features at spectral energies above around 2.0 eV being a linear combination of anisotropies in both Fe_3O_4 and γ-Fe_2O_3. Unfortunately, the lack of detailed optical measurements of γ-Fe_2O_3 across the probed spectral range prevents a systematic comparison between the spectra and a γ-Fe_2O_3 strain model.

The question arises as to what mechanism induces anisotropic shifts in energy of Fe_3O_4's bulklike states. Considering the likelihood of a γ-Fe_2O_3 overlayer, the response is discussed in terms of the strain gradients induced by a Fe_3O_4-γ-Fe_2O_3 interface. Such a strain gradient can induce small anisotropic shifts in energy of Fe_3O_4's optical transitions, producing a RAS signal comparable to the strain model below 2 eV, where Fe_3O_4 dominates. Progressive annealing, which reduces the magnitude of the derivativelike structure, likely progressively relieves the strain. For example, the magnitude of the RAS response of mechanically strained silicon is proportional to the applied strain [44]. At high temperatures in a UHV environment, for example, greater than ∼600 °C, a γ-Fe_2O_3 overlayer and a correlated RAS signal are not expected. This may explain the altered line shape after the 800 °C UHV anneal (Fig. 2, green dot-dashed line).

B. {111}-nanofaceted row reconstruction

1. RAS spectra

Annealing Fe_3O_4 in an UHV environment above ∼600 °C will transform a γ-Fe_2O_3 surface region to Fe_3O_4 [41]. The {111}-nanofaceted row reconstruction of Fe_3O_4 has been prepared by UHV flash annealing at 900 °C for 10 s. The corresponding STM and LEED measurements are depicted in Fig. 3. The LEED image shows a clean, well-ordered (1 × 3) row-reconstructed surface. The STM line profile illustrates that the reconstruction is characterized by a row periodicity of 25 Å along the [001] direction (which corresponds to three times the surface unit cell parameter along the [001] direction) and a step height of 3 Å [which corresponds to the interplanar distance between identical (110) planes, i.e., A plane to A plane or B plane to B plane]. These features are in agreement with the {111}-nanofaceted row reconstruction presented by Parkinson *et al.* [10].

Presented in Fig. 4 is the corresponding RAS measurement. The spectrum is characterized by a broad feature at high energies with peaks at 4.1 and 5.2 eV and a minima-maxima feature below around 2 eV. This derivativelike feature is similar to that of the as-polished crystal; however, there is a sign reversal. The dashed vertical lines in Fig. 4 depict Fe_3O_4's optical transitions, the same as those depicted in Fig. 2. In Fig. 4 the RAS spectrum is compared to the strain model with a value for d of 2.5 Å, chosen to match the minima-maxima feature in the infrared, which is well reproduced.

The comparison presented in Fig. 4 strongly indicates that the termination induces anisotropic energy shifts of bulklike states. The optical transitions which are modified in this energy regime are inter-Fe_{oct} sites, as below 2.0 eV optical transitions involve only these sites. In the case of the examined {111}-nanofaceted row reconstruction, the most likely explanation for the surface-induced modification of bulklike

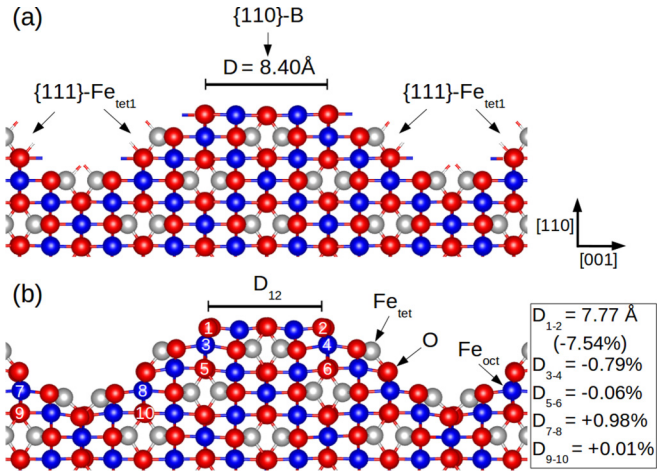

FIG. 5. (a) Initial and (b) relaxed geometries of the row-reconstruction model. Red, blue, and silver atoms correspond to oxygen, Fe_{oct}, and Fe_{tet}, respectively. Dangling bonds in the [001] direction are illustrated in (a). The black box provides examples of the percentages of compressive (negative) and tensile (positive) strain, relative to the bulk distance, within different layers. D_{1-2} corresponds to the distance between the two atoms labeled 1 and 2 in (b). Along the $[\bar{1}10]$ direction (into the page) no significant relaxations are observed. The calculation predicts an anisotropic strain gradient along the surface normal ([110] direction).

states is anisotropic strain. In the plane of the termination, the row reconstruction exhibits one-dimensional broken bonds. Fig. 5(a) aids in visualizing these broken bonds, which are in the [001] direction.

DFT calculations have been performed to examine whether this surface reconstruction induces a strain gradient. For full details of the calculation, the reader is directed to [45], as the parameters are identical. The model, which is depicted in Figure 5(a), corresponds to a stoichiometric Fe_3O_4 slab terminated by {111} Fe_{tet} and {110} B planes. This model is the same as that proposed by Parkinson *et al.* [10] in all aspects apart from the {110} termination. The atomic structure of this reconstruction remains an open question; the model in Fig. 5 is not suggested to resolve this question. However, the strain originates from the faceted nature of the reconstruction, and while the atomic structure will contribute to the spectra, which is demonstrated in the latter section of this work, it will not dictate whether the strain in present or not. Figures 5(a) and 5(b) depict the side-on initial and relaxed geometries. No significant relaxations along the $[\bar{1}10]$ direction (into the page) are present. The terminating layer sees significant relaxation along the [001] direction, and the immediately underlying layers see reducing relaxations in the [001] direction until the structure is bulklike. Therefore, the calculation predicts an anisotropic strain gradient. The ridge and trough sections of the unit cell see compressive and tensile strains, respectively. The interplanar distance for (110)-terminated Fe_3O_4 is 1.5 Å, and the DFT calculation predicts the strain is already close to zero after two layers and therefore 3 Å. Hence, this calculation provides confidence in the choice of $d = 2.5$ Å in the calculation of the RAS signal in Fig. 4.

Jeng and Guo have performed a DFT investigation of the influence of strain on bulk Fe_3O_4's electronic structure [46]. Uniaxial strain was applied in the [001] direction, the same direction which the DFT calculations in this work predict uniaxial strain in the terminating layers of the {111}-nanofaceted row reconstruction. It was found that under both compressive and tensile strains $Fe_{oct}(e_g)$ sites saw considerable modification, while other sites remained largely unchanged. Turning our attention to the optical transitions, the first transition involving a $Fe_{oct}(e_g)$ band occurs at 1.6 eV. This transition is between the $Fe^{2+}_{oct}(a_{1g})$ and $Fe^{2+}_{oct}(e_g)$ minority bands. In the energy range in which the experimental and calculated RASs are comparable (see Fig. 4) this transition is the only one involving a $Fe_{oct}(e_g)$ band. If the strain in the surface region modifies the minority $Fe_{oct}(e_g)$ band, it is reasonable to see good agreement between the experimental and calculated RAS signals in the vicinity of 1.6 eV.

Several broad transitions involving $Fe_{oct}(e_g)$ bands have been reported to occur beyond 2.0 eV, as depicted in Fig. 4. The broad feature observed experimentally in the ultraviolet may be related to strain-induced modification of $Fe_{oct}(e_g)$ bands. However, as previously stated, the three-phase derivative model is valid only for analyzing transitions around a single critical point.

2. *Modification of surface electronic structure*

In this section it is demonstrated that RAS is sensitive to the modification of the row reconstruction's surface structure, which is correlated to an altered stoichiometry in the surface region identified by XPS measurements.

During the XPS measurements, the $Fe_3O_4(110)$ single crystal was annealed in UHV and oxygen ($P_{O_2} = 3 \times 10^{-6}$ mbar) environments for 1.5 h at 800 °C, and the corresponding XPS spectra and LEED images are depicted in Fig. 6. Due to the lack of electron-beam heating, annealing in the XPS chamber is limited to ~800 °C. Therefore, the UHV annealing conditions differ from that which produced the surface depicted in Fig. 3, which was formed after flash annealing at ~900 °C. LEED provides the best means to compare and determine the state of the surface between the two chambers. The UHV annealed surface is indicative of the (1×3) {111}-nanofaceted row reconstruction, determined by the defined spots in the LEED image along the [001] direction. No defined spots are observed in the LEED of the oxygen-annealed crystal, indicating the surface is rougher and/or exhibits a lower degree of order. Therefore, of the two surfaces presented here, only the UHV-annealed crystal exhibits a well-ordered {111}-nanofaceted row reconstruction.

The different LEED patterns are correlated to different Fe $2p$ line shapes and stoichiometries in the surface region. The iron $2p_{3/2}$ and $2p_{1/2}$ peak positions of Fe_3O_4 are located at binding energies of 710.5 and 723 eV, respectively [47,48]. The Fe $2p_{3/2}$ peak is the sum of Fe^{2+} and Fe^{3+} components whose peaks reside at 708.5 and 710.5 eV, respectively [47–49]. Fe_3O_4 has a formal Fe^{3+}/Fe^{2+} ratio of 2; hence, the Fe $2p_{3/2}$ peak is positioned at the Fe^{3+} component, and a shoulder resides at the Fe^{2+} component [48]. As the Fe^{2+} content is reduced, the Fe $2p_{1/2}$ peak shifts to higher binding energies, with the peak residing at 724 eV for γ-Fe_2O_3, which contains

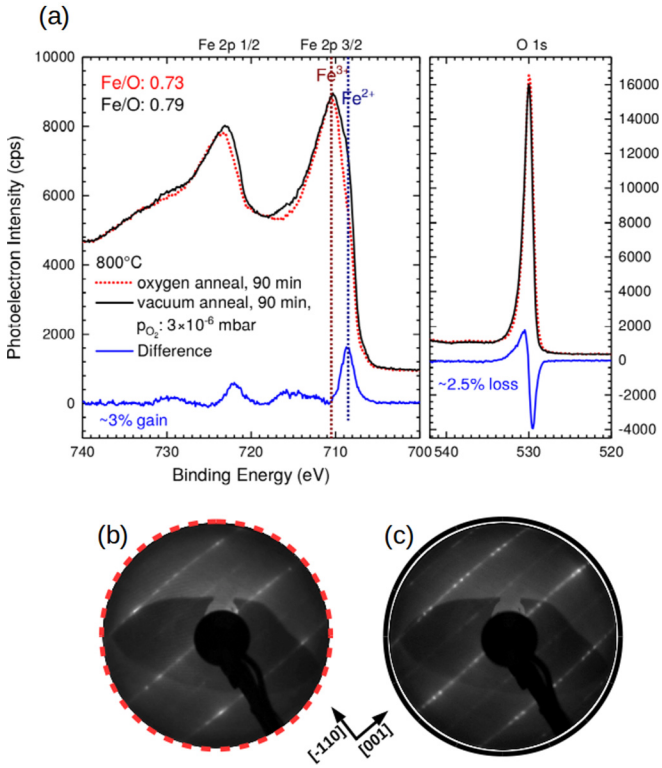

FIG. 6. (a) Dashed and solid curves represent the oxygen ($P_{O_2} = 3 \times 10^{-6}$ mbar) and UHV annealed crystal at a temperature of 800 °C for 1.5 h. The bottom curve represents the difference spectra, corresponding to the solid curve minus the dashed. The Fe $2p_{3/2}$ peak consists of Fe^{3+} and Fe^{2+} components whose energetic positions are represented by the vertical dashed lines. The Fe/O ratios of the UHV and oxygen annealed surface regions are calculated to be 0.79 and 0.73, respectively. The UHV annealed surface region exhibits a larger Fe^{2+}/Fe^{3+} ratio; this is best visualized by the peak at 708.5 eV in the difference spectra, which is located at the Fe^{2+} contribution to the Fe $2p_{3/2}$ peak. LEED images, obtained at 100 eV, indicate (c) the vacuum-annealed crystal (thick solid line) exhibits an ordered (1×3) row reconstruction, while (b) the oxygen-annealed crystal (red dashed line) exhibits a row reconstruction but with a weak degree of ordering.

zero Fe^{2+} ions [47]. Increased Fe^{2+} content sees the formation of a satellite peak at ∼716 eV, with a considerable feature present for Fe^{2+}-dominant $Fe_{1-x}O$ (wüstite) [48].

The spectra of the UHV- and oxygen-annealed surface regions correspond to raw counts without modification. The Fe/O ratios have been calculated by integrating the O 1*s* and Fe $2p_{3/2}$ peaks. The two peaks were fitted with three components each. The Fe/O ratio of the oxygen annealed crystal (Fig. 6, dashed line) is calculated to be 0.73, which is within the instrumental error of 0.75. Furthermore, the line shape is indicative of stoichiometric Fe_3O_4 [47,48].

The Fe/O ratio of the UHV-annealed crystal (solid line in Fig. 6) is calculated to be 0.79. What is important to note is the relative change in both the line shape and the Fe/O ratio compared to the stoichiometriclike surface (dashed line) and not the absolute magnitude of the Fe/O ratio. The Fe $2p$ core-level spectra exhibit three differences (highlighted by the difference line in Fig. 6) compared to the oxygen-annealed surface region: (1) The shoulder at 708.5 eV, at the Fe^{2+} contribution, is considerably larger. (2) In the range of 716 eV the onset of a satellite peak, which is observed in Fe^{2+}-dominant $Fe_{1-x}O$, is evident. (3) The $2p_{1/2}$ peak is shifted to a lower binding energy, which is also correlated to an increased Fe^{2+} content, as this peak shifts to *higher* binding energies for Fe^{2+}-free γ-Fe_2O_3. The O 1*s* line shape of the reduced termination is largely similar to that of the stoichiometric line shape, with only a minor shift to larger energy, which generates the derivativelike difference spectra. As in this work, this shift of the O 1*s* peak is reported to accompany the aforementioned changes in the Fe $2p$ line shape when $Fe_3O_4(001)$ is reduced via the deposition of iron [50].

It is important to note that the annealing environment alone will not dictate the surface structure, stoichiometry, and electronic properties. For example, sample history, annealing time, and temperature will influence such properties. These XPS measurements serve to highlight, first, that the {111}-nanofaceted row reconstruction is reduced and, second, that the annealing environment can relatively easily alter the stoichiometry and correlated iron valency in the surface region.

XPS and RAS measurements are performed in two different chambers, and hence, the crystal is exposed to atmospheric conditions in between measurements. RAS measurements are performed in the preparation section of the STM chamber. Therefore, scanning tunneling spectroscopy (STS) measurements can be utilized to probe the surface electronic structure of the reconstruction prepared under different conditions. In the STM chamber, the reconstruction has been prepared in both UHV [900 °C for 10 s, twice; Fig. 7(a)] and oxygen [850 °C, $P_{O_2} = 1 \times 10^{-6}$ for 5 min; Fig. 7(b)] environments. The two surfaces exhibit the {111}-nanofaceted row reconstruction, determined by STM line profiles and LEED images.

Grid spectroscopy measurements were performed on both of the presented terminations on areas similar to that of the STM images. At each individual spectroscopy point the tip height is determined by the constant-current mode scanning parameters, which are the same for the two grid spectroscopy measurements. The bias voltage is swept between +2 and −2 eV with the feedback loop switched off. At each individual point the spectrum is averaged over 10 individual current-voltage [$I(V)$] curves. The $dI(V)/dV$ curves are the numerical derivative of the $I(V)$ curves. Figures 7(c) and 7(d) depict the averaged (over ∼100 points on each grid) $I(V)$ curves and $dI(V)/dV$ curves of the {111}-nanofaceted row reconstruction of $Fe_3O_4(110)$ prepared in oxygen (dashed line) and UHV (solid line) environments. There is a clear inequivalence between the terminations, with the UHV- and oxygen-annealed prepared reconstructions exhibiting semiconducting gaps of ∼0.80 and ∼1.20 eV, respectively. Fe_3O_4 semiconducting surfaces are reported throughout the literature [37,50,51]. With the XPS measurements in mind, the altered surface electronic properties observed under different preparation conditions are suggested to result from different stoichiometries and correlated iron valencies in the surface region. It follows that this reconstruction is stable across some reduced stoichiometry range.

RAS measurements have been performed on the two terminations depicted in Fig. 7 to determine if RAS is sensitive to this change in surface structure. The two spectra depicted in

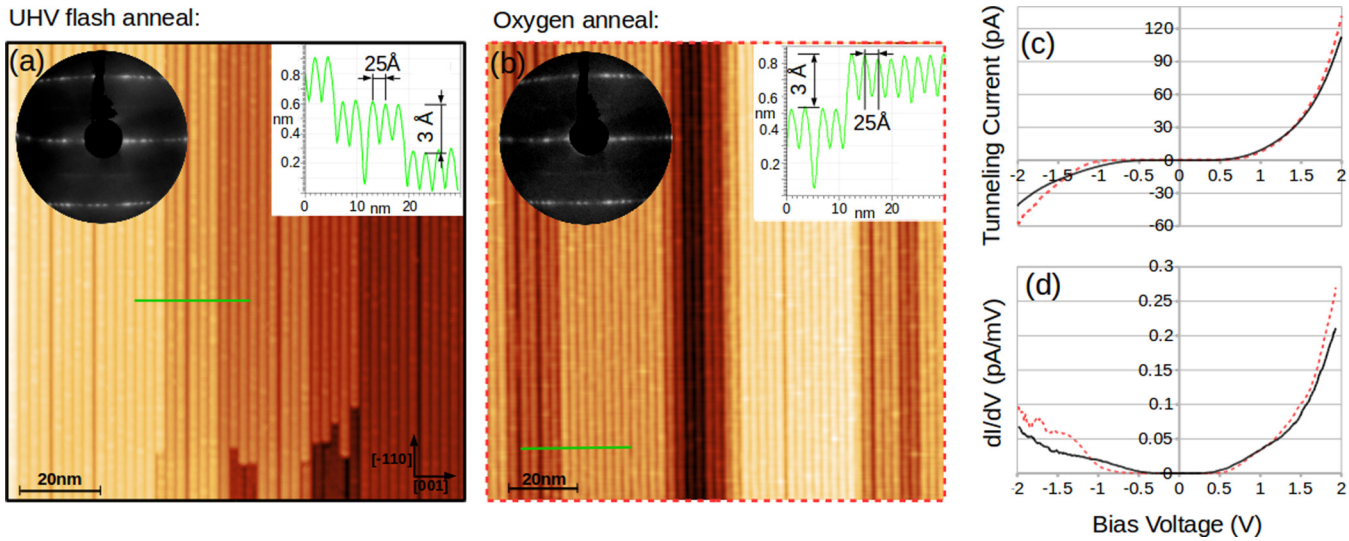

FIG. 7. (a) The 125 × 125 nm^2, $V = 1.2$ V, and $I = 87$ pA and (b) 140 × 140 nm^2, $V = 1.2$ V, and $I = 65$ pA STM images of the crystal prepared by UHV flash annealing (900 °C for 10 s, twice) and oxygen annealing (850 °C, $P_{O_2} = 1 \times 10^{-6}$ for 5 min). The LEED images and line profiles are indicative of the {111}-nanofaceted row reconstruction. Grid spectroscopy measurements have been performed on each of these surfaces. (c) and (d) depict the averaged $I(V)$ and $dI(V)/dV$ curves of the UHV (solid line) and oxygen (dashed line) prepared reconstructions. There is a clear inequivalence between the surface electronic structure, which is suggested to correlate to an altered stoichiometry and iron valency (see XPS measurements in Fig. 6) in the surface region induced by different preparation procedures.

Fig. 8 (dashed and solid lines) correspond to the oxygen and UHV prepared reconstructions. The spectra are very similar in shape; both exhibit the derivativelike feature below 2.0 eV and the broad feature and higher energies. This indicates the mechanism which generates the optical anisotropy is the same in each case. However, the magnitude of the features is larger in the case of the oxygen-annealed crystal.

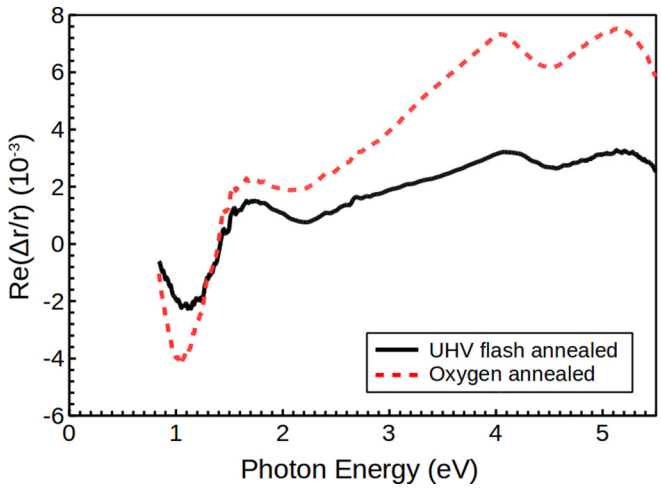

FIG. 8. RAS spectra of UHV-flash-annealed (solid line) and oxygen-annealed (dashed line) crystals, corresponding to the two surfaces depicted in Fig. 7, which exhibit different surface electronic properties. The line shapes are extremely similar, indicating the mechanism which generates the optical anisotropy is the same. However, the difference in magnitude of the prominent features highlights the two terminations are nonequivalent, which is suggested to result from different strain profiles correlated to different stoichiometries and iron valencies in the surface region.

Thus far, this spectrum has been interpreted to result from anisotropic strain in the terminating layers (see Fig. 4). Different strain profiles can increase or decrease the magnitude of a strain-induced response. The difference in magnitude of the RAS response of the {111}-nanofaceted row reconstruction prepared under different conditions is interpreted to be a result of different strain profiles in the terminating layers, induced by an altered stoichiometry in the surface region. The different strain profiles could be due to an altered depth of the strain [see Eq. (3)] and/or altered in-plane strain magnitudes.

V. DISCUSSION

The strain model used in this work provides qualitative analysis of the RAS spectra. Turning to Fig. 1, the polished surface is dominated by strain within Fe_3O_4 induced by a γ-Fe_2O_3-Fe_3O_4 interface [Fig. 1(b)] in the spectral region where one would not expect optical anisotropy within a γ-Fe_2O_3 termination [Fig. 1(a)] to contribute. Fe_3O_4's row-reconstructed termination is dominated by strain within Fe_3O_4 induced by the termination [Fig. 1(d)] in the infrared. Strain-induced optical anisotropy can induce multiple anisotropies, which can differ in width, sign, and magnitude. Hence, the strain model is not expected to provide quantitative analysis of the entire probed spectral range. Such analysis would require detailed knowledge of the strain-dependant dielectric function, which is available for only well-characterized materials (for example, silicon [52]). Direct contribution from the surface reconstruction [Fig. 1(c)], which can be expected due to its anisotropic nature, can be identified only by DFT calculations. The question of the atomic structure would have to resolved to correctly determine the contribution of the reconstruction. On the other hand, the presented RAS spectra can provide a means to determine the atomic structure as RAS is extremely sensitive to changes in atomic structure, as evidenced by Fig. 8 and

other studies of metal oxides [30]. These DFT calculations are out of the scope of the current work because simulating RAS spectra requires an accurate calculation of the band structure. This requires the inclusion of self-interaction terms [53] and a very large sampling of k space, which gives rise to a very computationally and time-consuming calculation.

The change in the row reconstruction's surface structure, specifically the stoichiometry and iron valency, is not observed by STM or LEED. The sensitivity of RAS, which is a noninvasive and relatively simple technique to employ during preparation, to the change in the row reconstruction's surface structure highlights its potential in monitoring the state of the surface in real time during preparation and, more importantly, during catalytic adsorption processes. More complex reconstruction changes, for example, due to absorbates during catalysis, are expected to lead to more dramatic changes. The sensitivity of RAS has been shown for other oxides [30], absorbates on silicon [26], and III-V semiconductor terminations [20,21].

VI. CONCLUSIONS

The RAS of the as-polished and row-reconstructed terminations of $Fe_3O_4(110)$ show a strong resemblance to the three-phase derivative model, indicating their responses originate from termination-induced anisotropic shifts in energy of bulk-like optical transitions. The optical anisotropy is concluded to originate from the anisotropic strain in the surface region. In the case of the as-polished surface, the strain is suggested to be related to a γ-Fe_2O_3 overlayer, which forms in the ambient. DFT calculations demonstrate that the Fe_3O_4's row reconstruction exhibits anisotropic strain in its terminating layers, which arises due to the faceted nature of this reconstruction.

XPS measurements highlight that (1) the stoichiometry and correlated iron valency of the $Fe_3O_4(110)$ surface region are relatively easily altered by the preparation procedure and (2) the {111}-nanofaceted row reconstruction is formed in reducing conditions. Moreover, STS measurements demonstrated that this reconstruction exhibits different electronic properties depending on the *in situ* preparation conditions, indicating the reconstruction is stable over some reduced range. RAS is shown to be sensitive to this change in surface structure, with the RAS magnitude being altered. This is suggested to be due to an altered strain profile induced by different surface region stoichiometries.

The sensitivity of RAS to the change in surface structure demonstrates this technique's potential to be employed during preparation and during catalytic absorption processes. Additionally, the comparison of the spectra to theory can provide a means to investigate the atomic structure of this reconstruction.

ACKNOWLEDGMENTS

This work was supported by Science Foundation Ireland through the Principal Investigator Grant (Grant No. 12/IA/1264). K.Z. would like to acknowledge the support of the Kazakh government under the Bolashak program.

[1] R. Arras, B. Warot-Fonrose, and L. Calmels, J. Phys.: Condens. Matter **25**, 256002 (2013).
[2] A. Yanase and N. Hamada, J. Phys. Soc. Jpn. **68**, 1607 (1999).
[3] E. J. W. Verwey, Nature (London) **144**, 327 (1939).
[4] J. P. Shepherd, J. W. Koenitzer, R. Aragón, C. J. Sandberg, and J. M. Honig, Phys. Rev. B **31**, 1107 (1985).
[5] F. P. D. Silva and L. M. Rossi, Tetrahedron **70**, 3314 (2014).
[6] D. S. Newsome, Catal. Rev.: Sci. Eng. **21**, 275 (1980).
[7] J. J. Richard, *Catalytic Ammonia Synthesis: Fundamentals and Practice* (Springer, New York, 2013).
[8] R. Bliem, E. McDermott, P. Ferstl, M. Setvin, O. Gamba, J. Pavelec, M. A. Schneider, M. Schmid, U. Diebold, P. Blaha, L. Hammer, and G. S. Parkinson, Science **346**, 1215 (2014).
[9] N. G. Condon, F. M. Leibsle, T. Parker, A. R. Lennie, D. J. Vaughan, and G. Thornton, Phys. Rev. B **55**, 15885 (1997).
[10] G. S. Parkinson, P. Lackner, O. Gamba, S. Maaß, S. Gerhold, M. Riva, R. Bliem, U. Diebold, and M. Schmid, Surf. Sci. **649**, L120 (2016).
[11] R. Bliem, R. Kosak, L. Perneczky, Z. Novotny, O. Gamba, D. Fobes, Z. Mao, M. Schmid, P. Blaha, U. Diebold *et al.*, ACS Nano **8**, 7531 (2014).
[12] R. Bliem, J. Pavelec, O. Gamba, E. McDermott, Z. Wang, S. Gerhold, M. Wagner, J. Osiecki, K. Schulte, M. Schmid, P. Blaha, U. Diebold, and G. S. Parkinson, Phys. Rev. B **92**, 075440 (2015).
[13] Z. Novotny, G. Argentero, Z. Wang, M. Schmid, U. Diebold, and G. S. Parkinson, Phys. Rev. Lett. **108**, 216103 (2012).
[14] K. T. Rim, D. Eom, S.-W. Chan, M. Flytzani-Stephanopoulos, G. W. Flynn, X.-D. Wen, and E. R. Batista, J. Am. Chem. Soc. **134**, 18979 (2012).
[15] X. Li and J. Paier, J. Phys. Chem. C **120**, 1056 (2016).
[16] G. S. Parkinson, Z. Novotny, P. Jacobson, M. Schmid, and U. Diebold, J. Am. Chem. Soc. **133**, 12650 (2011).
[17] R. Jansen, B. J. Nelissen, D. L. Abraham, H. van Kempen, and V. A. M. Brabers, IEEE Trans. Magn. **30**, 4506 (1994).
[18] G. Maris, O. Shklyarevskii, L. Jdira, J. G. H. Hermsen, and S. Speller, Surf. Sci. **600**, 5084 (2006).
[19] P. Weightman, D. S. Martin, R. J. Cole, and T. Farrell, Rep. Prog. Phys. **68**, 1251 (2005).
[20] J.-T. Zettler, Prog. Cryst. Growth Charact. Mater. **35**, 27 (1997).
[21] I. Kamiya, D. E. Aspnes, L. T. Florez, and J. P. Harbison, Phys. Rev. B **46**, 15894 (1992).
[22] T.-L. Chan, C. Z. Wang, M. Hupalo, M. C. Tringides, Z.-Y. Lu, and K. M. Ho, Phys. Rev. B **68**, 045410 (2003).
[23] J. R. Power, O. Pulci, A. I. Shkrebtii, S. Galata, A. Astropekakis, K. Hinrichs, N. Esser, R. Del Sole, and W. Richter, Phys. Rev. B **67**, 115315 (2003).
[24] A. Astropekakis, J. R. Power, K. Fleischer, N. Esser, S. Galata, D. Papadimitriou, and W. Richter, Phys. Rev. B **63**, 085317 (2001).
[25] D. S. Martin, A. M. Davarpanah, S. D. Barrett, and P. Weightman, Phys. Rev. B **62**, 15417 (2000).
[26] K. Fleischer, S. Chandola, N. Esser, W. Richter, and J. F. McGilp, Phys. Status Solidi A **188**, 1411 (2001).
[27] U. Rossow, R. Goldhahn, D. Fuhrmann, and A. Hangleiter, Phys. Status Solidi B **242**, 2617 (2005).
[28] K. Fleischer, R. Verre, O. Mauit, R. G. S. Sofin, L. Farrell, C. Byrne, C. M. Smith, J. F. McGilp, and I. V. Shvets, Phys. Rev. B **89**, 195118 (2014).

[29] S. Bahrs, A. Bruchhausen, A. R. Goñi, G. Nieva, A. Fainstein, K. Fleischer, W. Richter, and C. Thomsen, J. Phys. Chem. Solids **67**, 340 (2006).
[30] K. Fleischer, S. Kim, B. Walls, K. Zhussupbekov, and I. V. Shvets, Phys. Status Solidi B **255**, 1700459 (2017).
[31] J. D. E. McIntyre and D. E. Aspnes, Surf. Sci. **24**, 417 (1971).
[32] D. E. Aspnes, J. Vac. Sci. Technol., B: Microelectron. Process. Phenom. **3**, 1498 (1985).
[33] U. Rossow, L. Mantese, and D. E. Aspnes, Appl. Surf. Sci. **123–124**, 237 (1998).
[34] K. Fleischer, O. Mauit, and I. V. Shvets, Appl. Phys. Lett. **104**, 192401 (2014).
[35] R. Verre, K. Fleischer, C. Smith, N. McAlinden, J. F. McGilp, and I. V. Shvets, Phys. Rev. B **84**, 085440 (2011).
[36] R. Jansen, J. Vac. Sci. Technol., B: Microelectron. Nanometer Struct. Process., Meas., Phenom. **14**, 1173 (1996).
[37] R. Jansen, V. A. M. Brabers, and H. van Kempen, Surf. Sci. **328**, 237 (1995).
[38] S. F. A. A. Schlegel and P. Wachter, J. Phys. C **12**, 1157 (1979).
[39] V. N. Antonov, B. N. Harmon, V. P. Antropov, A. Y. Perlov, and A. N. Yaresko, Phys. Rev. B **64**, 134410 (2001).
[40] W. F. J. Fontijn, P. J. van der Zaag, M. A. C. Devillers, V. A. M. Brabers, and R. Metselaar, Phys. Rev. B **56**, 5432 (1997).
[41] G. Ketteler, W. Weiss, W. Ranke, and R. Schlögl, Phys. Chem. Chem. Phys. **3**, 1114 (2001).
[42] R. Grau-Crespo, A. Y. Al-Baitai, I. Saadoune, and N. H. D. Leeuw, J. Phys.: Condens. Matter **22**, 255401 (2010).
[43] M. I. Litter and M. A. Blesa, Can. J. Chem. **70**, 2502 (1992).
[44] D. Papadimitriou and W. Richter, Phys. Rev. B **72**, 075212 (2005).
[45] B. Walls, O. Lübben, K. Palotás, K. Fleischer, K. Walshe, and I. V. Shvets, Phys. Rev. B **94**, 165424 (2016).
[46] H.-T. Jeng and G. Y. Guo, Phys. Rev. B **65**, 094429 (2002).
[47] T. Fujii, F. M. F. de Groot, G. A. Sawatzky, F. C. Voogt, T. Hibma, and K. Okada, Phys. Rev. B **59**, 3195 (1999).
[48] T. Yamashita and P. Hayes, Appl. Surf. Sci. **254**, 2441 (2008).
[49] C. R. Brundle, T. J. Chuang, and K. Wandelt, Surf. Sci. **68**, 459 (1977).
[50] Z. Novotny, N. Mulakaluri, Z. Edes, M. Schmid, R. Pentcheva, U. Diebold, and G. S. Parkinson, Phys. Rev. B **87**, 195410 (2013).
[51] G. Maris, L. Jdira, J. G. H. Hermsen, S. Murphy, G. Manai, I. V. Shvets, and S. Speller, IEEE Trans. Magn. **42**, 2927 (2006).
[52] Z. Chong, M. Weisheit, M. Hecker, and E. Zschech, Semicond. Sci. Technol. **24**, 045013 (2009).
[53] W. G. Schmidt, F. Bechstedt, and J. Bernholc, J. Vac. Sci. Technol., B: Microelectron. Nanometer Struct. Process., Meas., Phenom. **18**, 2215 (2000).